Biosensors and Bioelectronics 73 (2015) 221–227

Contents lists available at ScienceDirect

Biosensors and Bioelectronics

journal homepage: www.elsevier.com/locate/bios

Amplified solid-state electrochemiluminescence detection of cholesterol in near-infrared range based on CdTe quantum dots decorated multiwalled carbon nanotubes@reduced graphene oxide nanoribbons

Juan Huan [1], Qian Liu [1], Airong Fei, Jing Qian, Xiaoya Dong, Baijing Qiu, Hanping Mao, Kun Wang *

Key Laboratory of Modern Agriculture Equipment and Technology, School of Chemistry and Chemical Engineering, Jiangsu University, Zhenjiang 212013, PR China

ARTICLE INFO

Article history:
Received 1 April 2015
Received in revised form
21 May 2015
Accepted 2 June 2015
Available online 9 June 2015

Keywords:
Amplified electrochemiluminescence
Near-infrared
CdTe quantum dot
Graphene nanoribbon
Solid-state cholesterol biosensor

ABSTRACT

An amplified solid-state electrochemiluminescence (ECL) biosensor for detection of cholesterol in near-infrared (NIR) range was constructed based on CdTe quantum dots (QDs) decorated multiwalled carbon nanotubes@reduced graphene nanoribbons (CdTe-MWCNTs@rGONRs), which were prepared by electrostatic interactions. The CdTe QDs decorated on the MWCNTs@rGONRs resulted in the amplified ECL intensity by ~4.5 fold and decreased onset potential by ~100 mV. By immobilization of the cholesterol oxidase (ChOx) and NIR CdTe-MWCNTs@rGONRs on the electrode surface, a solid-state ECL biosensor for cholesterol detection was constructed. When cholesterol was added to the detection solution, the immobilized ChOx catalyzed the oxidation of cholesterol to generate H_2O_2, which could be used as the co-reactant in the ECL system of CdTe-MWCNTs@rGONRs. The as-prepared biosensor exhibited good performance for cholesterol detection including good reproducibility, selectivity, and acceptable linear range from 1 μM to 1 mM with a relative low detection limit of 0.33 μM ($S/N=3$). The biosensor was successfully applied to the determination of cholesterol in biological fluid and food sample, which would open a new possibility for development of solid-state ECL biosensors with NIR emitters.

1. Introduction

Cholesterol, an essential lipid in the human organism, is an important biomarker for the management of many diseases, such as arteriosclerosis, myocardial infarction, brain thrombosis and etc. (Aravamudhan et al., 2007). Hence, it is extremely important for human health to develop efficient analytical methods for cholesterol content estimation. Although the traditional methods, including high performance liquid chromatography (Mariutti et al., 2008), spectrophotometric (Odo et al., 2013) and colorimetric (Li et al., 2012), are accurate for cholesterol determination, some methods often present certain disadvantages such as instability of reagents, poor specificity, expensive equipments or standardization difficulties (Hong et al., 2013). Due to the combination advantages of chemiluminescence (Shi et al., 2013) and electrochemistry (Li et al., 2011a), electrochemiluminescence (ECL) has attracted great attention in cholesterol determination by virtue of its unique advantages such as rapidity, high sensitivity, and simplified optical setup (Wu et al., 2014a; Wu et al., 2014b; Zhang et al., 2012; Zhang et al., 2014a). For example, using luminol as the ECL luminophor, Zhang et al. (2012) reported a cholesterol biosensor based on the catalytic activity of gold nanoparticles towards luminol–H_2O_2 system; Wu et al. (2014b) constructed an ECL biosensor for cholesterol detection based on the amplified ECL of luminol at the MWCNTs-GO-Thi-Au nanocomposites film. The results indicated that the resulting ECL biosensors above demonstrated high sensitivity and low detection limits for cholesterol detection. However, these ECL systems are solution-state, which would create high cost, large consumption of expensive ECL reagents and environmental pollution (Wang et al., 2014; Wei and Wang, 2008). Thus, it is urgent to immobilize the ECL luminophor on the electrode surface and explore solid-state ECL for cholesterol determination, which has been rarely reported to our knowledge.

Semiconductor quantum dots (QDs), on account of their high fluorescence quantum yields, stability against photo-bleaching, and size-controlled luminescence properties, have received tremendous attention in the fabrication of solid-state ECL systems (Bertoncello and Forster, 2009; Jiang et al., 2015; Stewart et al.,

* Corresponding author. Fax.: +86 511 88791708.
E-mail address: wangkun@ujs.edu.cn (K. Wang).
[1] These authors contributed equally to this work.

http://dx.doi.org/10.1016/j.bios.2015.06.004
0956-5663/

2015; Wei et al., 2013). To achieve efficient ECL of QDs for bioanalysis, it is an interesting approach for integrating QDs with carbon nanomaterials such as carbon nanotubes (CNTs) and graphene, which could not only amplified the ECL intensity but also reduced the over-potential of ECL systems (Chen et al., 2011; Li et al., 2011b; Wang et al., 2009, 2010). For example, in situ growth of CdS QDs on the wall of CNTs could enhance the ECL intensity of QDs and move the onset ECL potential positively (Wang et al., 2009); the CdSe QDs–graphene composite exhibited amplified ECL signal and decreased potential barriers of the ECL reduction due to the extraordinary electron transport of the doped graphene (Li et al., 2011b); the addition of nitrogen-doped graphene (NG) in the NG/CdTe QDs composite resulted in the improved ECL property of CdTe QDs tremendously (Zhang et al., 2014b). All these result above indicated that the ECL property of QDs could be improved effectively by the incorporation of carbon nanomaterials, which showed grand potential in the fabrication of ECL sensing interface with good performance.

Recently, with the development of synthetic strategies of near-infrared (NIR) emitters, great efforts have been involved in ECL strategies with NIR QDs, as NIR emission between 650 and 900 nm offers several advantages in actual biological analysis such as improved tissue penetration, lower background interference, and reduced photochemical damage (Cui et al., 2012; Smith et al., 2009; Wang and Han, 2013). In this work, CdTe QDs decorated multiwalled carbon nanotubes@reduced graphene nanoribbons (CdTe-MWCNTs@rGONRs) with NIR ECL property were prepared by electrostatic interactions, which showed amplified ECL intensity and decreased onset potential than that of pure CdTe QDs. And further, a solid-state ECL enzyme biosensor for cholesterol detection in NIR range was constructed by immobilization of the cholesterol oxidase (ChOx) and NIR CdTe-MWCNTs@rGONRs on the electrode surface. The resulting solid-state biosensor was successfully applied to the determination of cholesterol in biological fluid and food sample with satisfactory recovery, which provided a promising alternative on the design of the solid-state NIR ECL bioassays.

2. Experimental

2.1. Materials

3-Mercaptopropionic acid (MPA) modified CdTe QDs were prepared according to the literature (Weng et al., 2006). Tellurium powder, $CdCl_2 \cdot 2.5H_2O$, $NaBH_4$, cholesterol, H_2O_2, isopropanol and Triton X-100 were obtained from Sinopharm Chemical Reagent Co. Ltd. (Shanghai, China). MPA and ChOx were purchased from Sigma-Aldrich (USA). Phosphate buffered solution (PBS, 0.10 M) of various pH values was prepared by mixing stock standard solutions of NaH_2PO_4 and Na_2HPO_4, and adjusted the pH with 0.10 M NaOH or H_3PO_4 solution. A stock solution of cholesterol was prepared by dissolving cholesterol in the mixture of isopropanol and Triton X-100 (1:1, v/v) and the standard cholesterol solutions were diluted with the as-prepared PBS (pH 7.0) and then stored at 4 °C. All the reagents were used as purchased without further purification. Double-distilled water was used throughout the study.

2.2. Apparatus

Transmission electron microscopy (TEM) image was taken with a JEOL 2100 transmission electron microscopy (JEOL, Japan) operated at 200 kV. The UV–vis absorption spectra were measured by an UV-2450 spectrophotometer (Shimadzu, Japan) and fluorescence spectra were recorded on a Hitachi F-4500 fluorescence spectrophotometer (Tokyo, Japan). Raman spectra of the samples were obtained from a RM 2000 microscopic confocal Raman spectrometer (Renishaw, England). X-ray photoelectron spectrometry (XPS) analyses were carried out on an ESCALAB MKII X-rayphotoelectron spectrometer (V.G. Scientific. Ltd, England). The electrochemical impedance spectroscopy (EIS) was performed with a ZENNIUM electrochemical workstation (Zahner Instruments, Germany) in 0.10 M KCl solution containing 5 mM $Fe(CN)_6^{3-/4-}$. The ECL curves were recorded by a Model MPI-A ECL analyzer system (Xi'An Remax Electronic Science and Technology Co. Ltd., Xi'An, China). The photomultiplier tube was biased at 800 V in the ECL process. The ECL spectrum of the CdTe-MWCNTs@rGONRs was detected by a series of high-energy optical filters (640, 660, 680, 700, 720, 740 and 760 nm) from Omega Optical Inc., USA. All cyclic voltammetric (CV) and ECL curves were recorded with a conventional three-electrode system where a glassy carbon electrode (GCE, 3 mm in diameter) was used as working electrode, a Ag/AgCl (saturated KCl solution) as reference electrode and platinum wire as counter electrode.

2.3. Preparation of CdTe-MWCNTs@rGONRs composites

The CdTe-MWCNTs@rGONRs composites were prepared via electrostatic interactions between negatively charged MPA modified CdTe QDs and positively charged MWCNTs@rGONRs, which was noncovalently functionalized with PDDA, as displayed in Scheme 1. Firstly, the MWCNTs@GONRs were synthesized from MWCNTs according to our previous report (Liu et al., 2015) due to the presence of the oxygen-containing functional groups such as –COOH on the surface of MWCNTs@GONRs, the MWCNTs@GONRs exhibited better stability and dispersibility in water than MWCNTs. Then, the PDDA–MWCNTs@rGONRs was prepared via the in situ reduction of MWCNTs@GONRs in the presence of PDDA. In details, 0.5 mL 20% PDDA containing 0.5 M NaCl was added to 100 mL 0.5 mg/mL MWCNTs@GONRs solution and stirred for 30 min; then 0.5 mL 80% hydrazine hydrate was added and stirring maintained for 24 h at 90 °C. The black suspension of PDDA–MWCNTs@rGONRs could be obtained by suction filtration and washing with distilled water, and then re-dispersed in water for use. Due to electrostatic repulsion, the obtained solution dispersion possessed good separation and stability. Finally, PDDA–MWCNTs@rGONRs were mixed with CdTe QDs solution under sonication for 30 min.

2.4. Fabrication of the ChOx/CdTe-MWCNTs@rGONRs modified electrode and its detection mechanism towards cholesterol

Prior to modification, the GCE was first polished with sand paper followed by 1.0, 0.3, and 0.05 μm alumina slurry. After successive sonication in ethanol and double distilled water, the electrode was rinsed with double distilled water and allowed to dry at room temperature.

As displayed in Scheme 1, the modified electrode was prepared by a simple casting method as follows: initially, the pretreated GCE was modified by dropping 6 μL of 1 mg mL^{-1} CdTe-MWCNTs@GONRs/water solution and drying (denoted as CdTe-MWCNTs@GONRs/GCE); then the obtained electrode was coated with 10 μL ChOx solutions (50 U mL^{-1}) to form ChOx/CdTe-MWCNTs@GONRs/GCE. After evaporation of water, the modified electrode was washed with 0.1 M PBS to remove the unbound ChOx, and the resulting GCE was stored at 4 °C when not use.

The principle of the biosensor is as follows: As shown in Scheme 1, in the absence of analyte cholesterol, only very weak ECL signal was detected on the biosensor. After cholesterol was added into the solutions, the ChOx immobilized on the modified electrode could catalyze the oxidation of cholesterol to produce H_2O_2, which could be used as the co-reactant for amplified the ECL

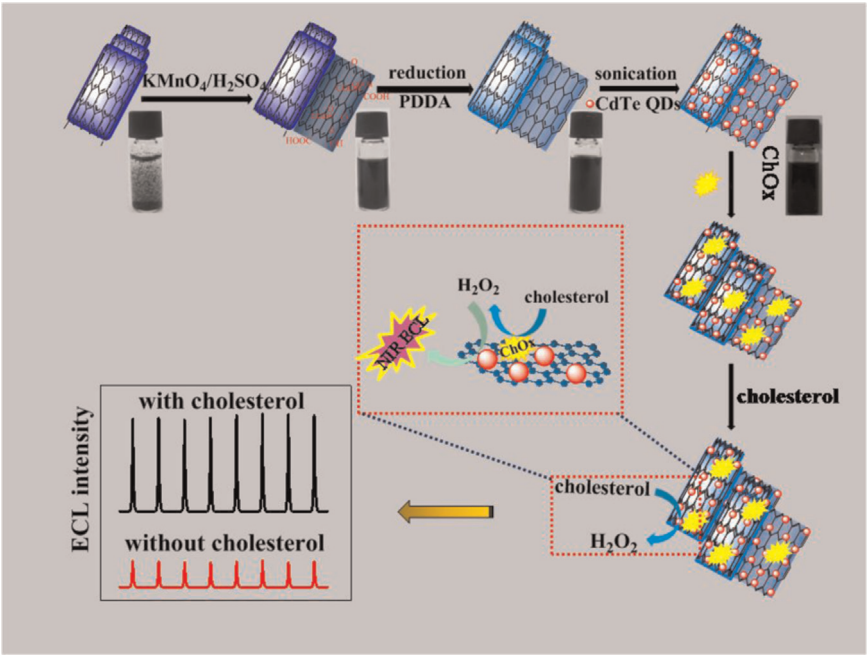

Scheme 1. The schematic presentation for controllable preparation of NIR CdTe-MWCNTs@rGONRs for solid-state ECL cholesterol biosensor fabrication and its detection mechanism.

signals of the biosensor (Han et al., 2007). The logarithm of cholesterol concentration increases in proportion to the ECL intensity; thus, cholesterol can be detected quantitatively on the modified electrode.

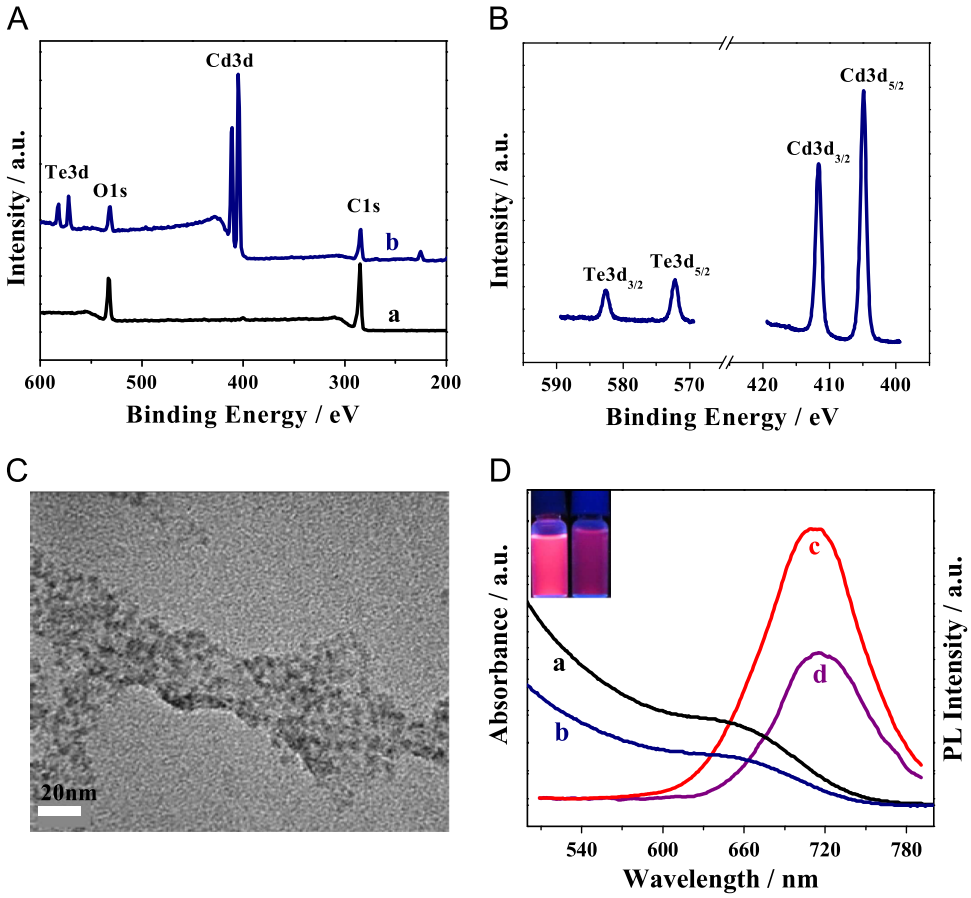

Fig. 1. (A) XPS survey scan of MWCNTs@GONRs (a) and CdTe-MWCNTs@rGONRs (b); (B) Cd 3d and Te 3d spectrum of CdTe-MWCNTs@rGONRs; (C) TEM images of CdTe-MWCNTs@rGONRs; (D) The UV–vis absorption and fluorescence spectra of pure CdTe QDs (a, c) and CdTe-MWCNTs@rGONRs (b, d). Inset: the corresponding photographs of pure CdTe QDs (left) and CdTe-MWCNTs@rGONRs (right) under a UV lamp (λ_{ex}=365 nm). (For interpretation of the references to color in this figure, the reader is referred to the web version of this article.)

3. Results and discussion

3.1. Characterization of the PDDA–MWCNTs@rGONRs

The UV–vis absorption spectra of MWCNTs@GONRs and PDDA–MWCNTs@rGONRs are shown in Fig. S1A. For the MWCNTs@GONRs, a typical absorption peak at ~235 nm corresponded to the $\pi \rightarrow \pi^*$ transition of C=C was observed (Luo et al., 2009). For comparison, the corresponding absorption peak in the spectrum of PDDA–MWCNTs@rGONRs was red-shift to ~255 nm, indicating that the MWCNTs@GONRs were reduced in the reaction process (Shin et al., 2009). The formation of defects in carbonaceous materials was monitored by the ratio of the intensities of D and G bands (I_D/I_G) in the Raman spectrum. The similar characteristic D and G bands were obtained at MWCNTs@GONRs and PDDA–MWCNTs@rGONRs with the I_D/I_G values of 0.81 and 0.95 (Fig. S1B), and the increased I_D/I_G of PDDA–MWCNTs@rGONRs suggested the MWCNTs@GONRs was reduced effectively by hydrazine hydrate in the reaction process (Yeh et al., 2014).

3.2. Characterization of the CdTe-MWCNTs@rGONRs composites

The XPS measurements were carried out to prove the formation of CdTe-MWCNTs@rGONRs. The survey analysis showed the peaks of the elements present in the MWCNTs@GONRs and CdTe-MWCNTs@rGONRs. The C 1s peak at 285.5 eV and O 1s peak at 532.4 eV were observed in the spectrum of MWCNTs@GONRs (Fig. 1A) (Vennerberg et al., 2014). Except for the characteristic peaks above, the appearance of a characteristic Cd $3d_{5/2}$ peak at 404.8 eV and Te $3d_{5/2}$ peak at 572.2 eV was observed at the CdTe-MWCNTs@rGONRs (Fig. 1B), which confirmed the existence of cadmium and tellurium in the CdTe-MWCNTs@rGONRs and the composite of CdTe-MWCNTs@rGONRs was formed (Zhang et al., 2003). The morphology of the MWCNTs@GONRs and CdTe-MWCNTs@rGONRs was investigated by TEM. The TEM image of MWCNTs@GONRs exhibited the GONRs structures appear on the side of nanotubes, meanwhile the central cores of nanotubes remained tube-like structure (Fig. S2). For comparison, the TEM image of CdTe-MWCNTs@rGONRs displayed in Fig. 1C showed the CdTe QDs (dark spots) were well dispersed on the surface of MWCNTs@rGONRs (gray basement).

Moreover, the UV–vis absorption and fluorescence spectra of pure CdTe QDs and CdTe-MWCNTs@rGONRs are compared in Fig. 1D. The absorption maximum at 660 nm (curve a) of the pure CdTe QDs indicates the consequence of quantum confinement. In the absorption spectrum of CdTe-MWCNTs@rGONRs (curve b), no obvious change of the absorption peak was observed, indicated that almost no CdTe QDs agglomerate was formed on the surface of MWCNTs@rGONRs, which is consistent with the TEM observations. However, by comparing the fluorescence spectrum of CdTe-MWCNTs@rGONRs (curve d) with pure CdTe QDs (curve c) in Fig. 1D, a slight red-shift (5 nm) was observed. Besides, a dramatic decrease in fluorescence intensity was found compared with that of CdTe QDs, which indicates the partial quenching due to the photoinduced electrons transfer from excited CdTe QDs to MWCNTs@rGONRs (Li et al., 2011b). The corresponding photographs of CdTe QDs (left) and CdTe-MWCNTs@rGONRs (right) under UV illumination are presented in the inset of Fig. 1D; it is obvious that the red color of CdTe-MWCNTs@rGONRs was darker than that of CdTe QDs. This result vividly showed that the fluorescence performance of CdTe QDs was partial quenched by the MWCNTs@rGONRs, which was consistent with the fluorescence spectra in Fig. 1D.

3.3. Electrochemical and ECL behaviors of the CdTe-MWCNTs@rGONRs

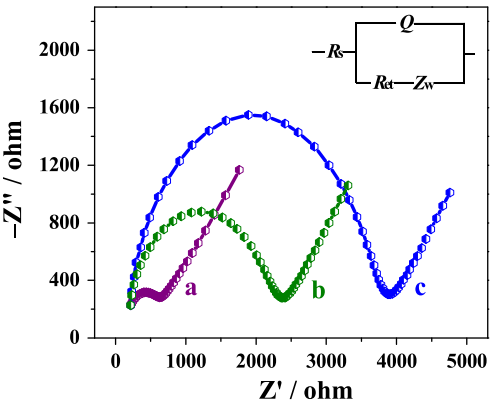

Fig. 2. EIS of bare GCE (a), CdTe-MWCNTs@rGONRs/GCE (b) and ChOx/CdTe-MWCNTs@rGONRs/GCE (c) in 0.10 M KCl containing 5.0 mM $Fe(CN)_6^{3-/4-}$.

Electrochemical impedance spectroscopy (EIS) is an effective method for monitoring the changes in the surface features of the modified electrodes in the assembly process. The semicircle diameter of impedance is equal to the electron transfer resistance (R_{et}), which controls the electron transfer kinetics of the redox probe at the electrode interface. Fig. 2 illustrates the impedance spectra of each modified stage in 0.10 M KCl containing 5.0 mM $Fe(CN)_6^{3-/4-}$. Compared with bare GCE (curve a), R_{et} of CdTe-MWCNTs@rGONRs/GCE (curve b) was increased, indicated that CdTe-MWCNTs@rGONRs was successful immobilized on the GCE. After the ChOx was coated onto the electrode, R_{et} was further increased (curve c) due to the non-conductive ChOx obstructed electron transfer (Zhang et al., 2014b; Zhang et al., 2014a), which was the direct evidence of successful modification of ChOx on the electrode surface.

The electrochemical behaviors of the bare GCE, CdTe QDs/GCE and CdTe-MWCNTs@rGONRs/GCE were investigated in the potential range scanned from 0 to −1.7 V in 0.10 M N_2-saturated PBS (pH 9.0). As shown in Fig. S3, no obvious redox current was found at bare GCE (curve a), and a pair of redox peaks at ca. −0.82 and −1.1 V at CdTe/GCE (curve b) and CdTe-MWCNTs@rGONRs/GCE (curve c) were observed, which were ascribed to the oxidation and reduction of CdTe QDs (Amelia et al., 2012). Furthermore, the redox peak current at CdTe-MWCNTs@rGONRs was much larger than that of CdTe/GCE, indicating that the MWCNTs@rGONRs in the CdTe-MWCNTs@rGONRs composites could facilitate the electrochemical redox process of CdTe QDs (Li et al., 2011b). When 50.0 μM H_2O_2 was added into the solution, the redox peak currents at both CdTe QDs and CdTe-MWCNTs@rGONRs film increased (Fig. 3A), which was due to the electrocatalytic reaction between CdTe QDs and H_2O_2 (Wang et al., 2009; Wang et al., 2010).

During the ECL experiments, the ECL curves of bare GCE (a), CdTe QDs/GCE (b) and CdTe-MWCNTs@rGONRs/GCE (c) were studied in 0.10 M PBS (pH 9.0) with the co-reactant of 50.0 μM H_2O_2. As shown in Fig. 3B, no light emission was detected from bare GCE; under the same condition, light emission was occurred from CdTe QDs/GCE (b) and CdTe-MWCNTs@rGONRs/GCE (c), indicated that the ECL peak was produced by the catalytic reaction between CdTe QDs and H_2O_2, and the ECL mechanism of the catalytic reaction is as follows (Ding et al., 2006; Ding et al., 2012):

$$\text{CdTe QD} + e^- \rightarrow \text{CdTe QD}^{-*}$$

$$\text{CdTe QD}^{-*} + H_2O_2 \rightarrow \text{CdTe QD}^{*} + OH^-$$

$$\text{CdTe QD}^{*} \rightarrow \text{CdTe QD} + h\nu$$

In addition, the ECL intensity of CdTe-MWCNTs@rGONRs film was increased ~4.5 times over that of CdTe QDs, and the ECL onset

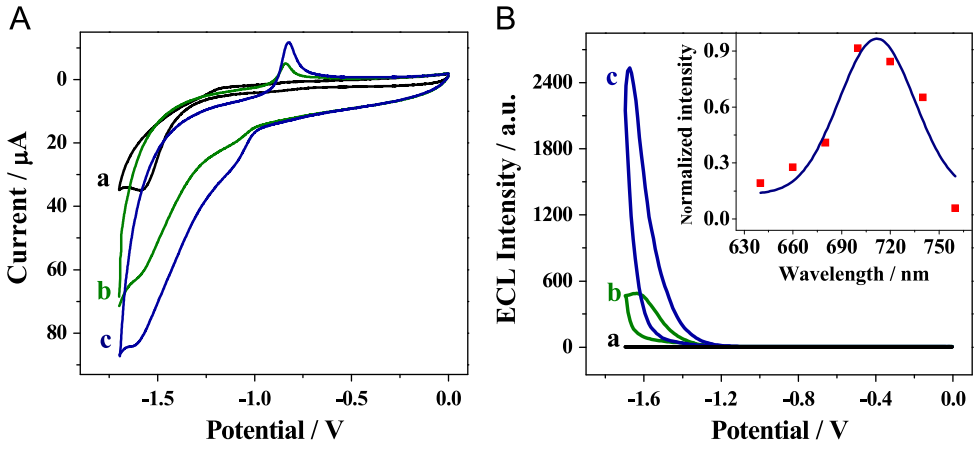

Fig. 3. (A) CV and (B) ECL–potential curves of bare GCE (a), CdTe QDs/GCE (b) and CdTe-MWCNTs@rGONRs/GCE (c) in 0.10 M PBS (pH 9.0) with 50.0 μM H_2O_2. Inset: ECL spectrum of CdTe-MWCNTs@rGONRs.

potential of CdTe-MWCNTs@rGONRs modified electrode was positively shifted for ~100 mV than that of CdTe QDs. This fact suggested that the MWCNTs@rGONRs in the CdTe-MWCNTs@rGONRs could enhance the ECL intensity of CdTe QDs and decrease the ECL onset potential effectively.

The ECL spectrum of the CdTe-MWCNTs@rGONRs film was also investigated in 0.10 M PBS (pH 9.0) with the co-reactant H_2O_2. As displayed in Fig. 3B inset, the ECL spectrum of CdTe-MWCNTs@rGONRs film demonstrated a maximum wavelength around 711 nm, which was almost identical to that in the fluorescence spectrum of CdTe QDs. The fact demonstrated that the strong ECL signals were certainly located in NIR range and resulted from the original CdTe QDs (Li et al., 2013).

3.4. ECL behavior of ChOx/CdTe-MWCNTs@rGONRs/GCE

On the basis of the above good ECL properties of the as-prepared CdTe-MWCNTs@rGONRs film, a NIR ChOx biosensor was further constructed for the indirect quantification of cholesterol by the determination of the H_2O_2 product obtained from cholesterol oxidation. As expected, the addition of cholesterol resulted in a significant increase in the ECL intensity of ChOx/CdTe-

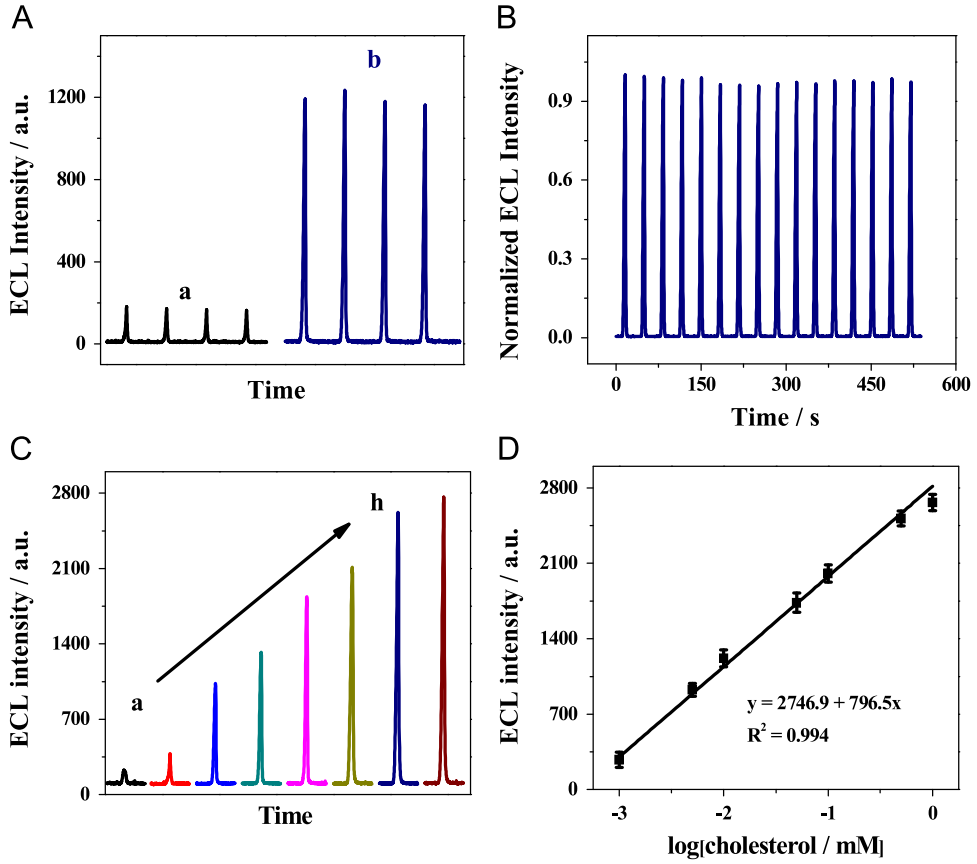

Fig. 4. (A) ECL responses of ChOx/CdTe-MWCNTs@rGONRs/GCE in 0.10 M PBS (pH 9.0) in the absence (a) and presence (b) of 10.0 μM cholesterol; (B) ECL emission from ChOx/CdTe-MWCNTs@rGONRs/GCE in 0.10 M PBS (pH 9.0) containing 10.0 μM cholesterol under continuous cyclic scans from 0 to −1.7 V for 16 cycles; (C) ECL responses of ChOx/CdTe-MWCNTs@rGONRs/GCE in 0.10 M PBS (pH 9.0) in the presence of 0 (a), 0.001 (b), 0.005 (c), 0.01 (d), 0.05 (e), 0.1 (f), 0.5 (g), and 1.0 mM (h) cholesterol; (D) the calibration curve for cholesterol detection.

Table 1
Comparison of the analytical properties of different cholesterol assays.

Materials	Method	Linear range (μM)	Detection limit (μM)	References
ChOx–CS[a]/Hb[b]–CS	Chronoamperometry	10–600	9.5	Zhao et al. (2008)
(PDDA–[MWCNTs–ChOx]$_5$)	CV	200–1000	30	Manjunatha et al. (2011)
[PSS[c]/PEI[d]/COX]$_n$	CV	50–1000	Not given	Ram et al. (2001)
ChOx/L-cys-rGO[e] composites	ECL	3.3–1000	1.1	Zhang et al. (2012)
CdSeTe/ZnS core–shell QD–chitosan–ChOx	ECL	250–5000	Not given	Stewart et al. (2015)
ChOx/poly(luminol-biotinylated pyrrole)	ECL	15–800	14.7	Ballesta-Clavera et al. (2012)
ChOx/CdTe-MWCNTs@rGONRs	ECL	1–1000	0.3	This work

[a] CS, chitosan.
[b] Hb, hemoglobin.
[c] PSS, poly(styrene sulfonate).
[d] PEI, poly(ethylene imine).
[e] L-cys-rGO L-cysteine-reduced graphene oxide.

MWCNTs@rGONRs/GCE (Fig. 4A), which was due to that the cholesterol could be catalyzed by the immobilized ChOx to produce H_2O_2. This result indicated that the NIR ECL platform could be used for cholesterol monitoring effectively.

Fig. 4B displayed the ECL behavior of ChOx/CdTe-MWCNTs@rGONRs/GCE in 0.10 M PBS (pH 9.0) containing 10.0 μM cholesterol under continuous cyclic scans from 0 to −1.7 V for 16 cycles. No obvious change was observed when the ECL response was repeated under continuous cyclic scans, suggested that the current ECL detection method showed good stability for the cholesterol determination, which was beneficial for the construction of the ECL biosensor.

3.5. Effect of solution pH value on the ECL intensity of the biosensor

In order to achieve the optimal ECL response for cholesterol determination, the effect of solution pH value from 6.0 to 11.0 on the performance of ECL biosensor was investigated. As can be seen from Fig. S4, the ECL intensity increased with increasing pH and the greatest ECL intensity was obtained at pH 9.0. Thus, pH 9.0 was selected as the detection solution in this experiment.

3.6. Cholesterol detection based on the NIR ECL biosensor

Under the optimal experimental condition, the fabricated NIR ECL biosensor was evaluated by detecting standard cholesterol solutions with the purpose of quantitative analysis of cholesterol. As shown in Fig. 4C, the ECL intensity increased accordingly with the increasing of cholesterol concentration. The ECL signal (Fig. 4D) showed a linear range from 1 μM to 1 mM with a low detection limit of 0.33 μM ($S/N=3$), and the corresponding calibration equation was $I_{ECL}=2746.9+796.5x$ with a correlation coefficient $R^2=0.994$. Furthermore, the performance of the proposed ECL biosensor was compared with those cholesterol assays reported in the literatures in Table 1. It could be observed that the proposed biosensor had a comparative or relative wide linear range and low detection limit, which might be attributed to the effectively amplified ECL using in situ generated H_2O_2 as the co-reactant for CdTe QDs under the amplification of MWCNTs@rGONRs.

3.7. Selectivity, reproducibility, stability of the biosensor

Selectivity, reproducibility and stability are important factors for evaluating the performance of the biosensor. To confirm the selectivity of the proposed ChOx biosensor, some molecules (dopamine, uric acid, ascorbic acid and glucose) and inorganic ions (Na^+, K^+, Mg^{2+}, Ca^{2+}, SO_4^{2-}, PO_4^{3-}, and Cl^-) that co-exist with cholesterol in food samples were used as the sources of interferences. As shown in Fig. S5, the ECL signals change to successive additions of 50.0 μM of these substances were not noticeable for the detection of 10.0 μM cholesterol. It suggests that the selectivity of the biosensor was acceptable. The reproducibility of the analytical responses was obtained from different electrodes constructed by the same procedure with a relative standard deviation (RSD) of 7.8%. While 5 measurements for a single electrode were made upon the addition of 10.0 μM cholesterol in 0.10 M PBS (pH 9.0) with RSD of 4.9%, demonstrating excellent reproducibility of the biosensor. The stability of the biosensor was also determined by measuring change in the ECL response at regular interval of 3 days for 3 weeks. The ECL response decreased to 91.6% after 1 week and 81.3% after 3 weeks. These results indicated that the proposed biosensor had good selectivity, reproducibility and stability.

3.8. Real sample analysis

In order to check the applicability and feasibility of this sensor, it was applied to determinate of cholesterol in commercial milk and human serum samples. The milk and human serum samples were pretreated according to the previous reports (Daneshfar et al., 2009; Ruecha et al., 2014), and then the standard addition experiments were performed to evaluate the practical applicability of the proposed method. The cholesterol content of the milk samples and diluted human serum samples is listed in Table S1. It was found that the recoveries of the spiked milk samples and human serum samples were between 93.4% and 104.9% with the RSD less than 6.0%, verifying that this sensing system is reliable for detection of cholesterol in real samples.

4. Conclusions

The NIR CdTe-MWCNTs@rGONRs was prepared by electrostatic interactions, which exhibited the amplified ECL intensity and decreased ECL onset potential than that of pure CdTe QDs. Based on the immobilization of NIR CdTe-MWCNTs@rGONRs and ChOx on the electrode surface, a solid-state ECL cholesterol biosensor was constructed, which showed good performance for cholesterol detection in the advantages of good reproducibility, selectivity, acceptable linear range and relative low detection limit. The proposed solid-state ECL biosensor opened a new way for designing a novel NIR ECL reagent with practical applications in clinical diagnosis and biotechnology.

Acknowledgments

The present work was supported by the National Natural Science Foundation of China (Nos. 21175061, 21305052, 21375050

and 21405063), Key Laboratory of Modern Agriculture Equipment and Technology (No. NZ201109), Innovation Project of Science and Technology for Graduates of Jiangsu University (No. KYXX_0023), Project Funded by Qing Lan and the Priority Academic Program Development of Jiangsu Higher Education Institutions (No. PAPD-2014-37).

Appendix A. Supplementary material

Supplementary data associated with this article can be found in the online version at http://dx.doi.org/10.1016/j.bios.2015.06.004.

References

Amelia, M., Lincheneau, C., Silvi, S., Credi, A., 2012. Chem. Soc. Rev. 41, 5728–5743.
Aravamudhan, S., Ramgir, N.S., Bhansah, S., 2007. Sens. Actuators B 127, 29–35.
Ballesta-Claver, J., Ametis-Cabello, J., Morales-Sanfrutos, J., Megía-Fernández, A., Valencia-Mirón, M.C., Santoyo-González, F., Capitán-Vallvey, L.F., 2012. Anal. Chim. Acta 754, 91–98.
Bertoncello, P., Forster, R.J., 2009. Biosens. Bioelectron. 24, 3191–3200.
Chen, Y., Shen, Y.Y., Sun, D., Zhang, H.Y., Tian, D.B., Zhang, J.R., Zhu, J.J., 2011. Chem. Commun. 47, 11733–11735.
Cui, R., Gu, Y.P., Bao, L., Zhao, J.Y., Qi, B.P., Zhang, Z.L., Xie, Z.X., Pang, D.W., 2012. Anal. Chem. 84, 8932–8935.
Daneshfar, A., Khezeli, T., Lotfi, H.J., 2009. J. Chromatogr. 877, 456–460.
Ding, S.N., Xu, J.J., Chen, H.Y., 2006. Chem. Commun. 34, 3631–3633.
Ding, S.N., Gao, B.H., Shan, D., Sun, Y.M., Cosnier, S., 2012. Chem. Eur. J. 18, 1595–1598.
Han, H.Y., Sheng, Z.H., Liang, J.G., 2007. Anal. Chim. Acta 596, 73–78.
Hong, L., Liu, A.L., Li, G.W., Chen, W., Lin, X.H., 2013. Biosens. Bioelectron. 43, 1–5.
Jiang, D., Du, X.J., Liu, Q., Zhou, L., Qian, J., Wang, K., 2015. ACS Appl. Mater. Interfaces 7, 3093–3100.
Li, F., Li, J.J., Feng, Y., Yang, L.M., Du, Z.F., 2011a. Sens. Actuators B 157, 110–114.
Li, L.L., Liu, K.P., Yang, G.H., Wang, C.M., Zhang, J.R., Zhu, J.J., 2011b. Adv. Funct. Mater. 21, 869–878.
Li, L.L., Shen, Y.Y., Xu, M., Ji, J., Lu, Q., Fei, R., Zhang, K., Zhang, J.R., Zhu, J.J., 2013. Sci. Rep. 3, 1529.
Li, R., Xiong, C., Xiao, Z., Ling, L., 2012. Anal. Chim. Acta 724, 80–85.
Liu, Q., Huan, J., Fei, A.R., Mao, H.P., Wang, K., 2015. Talanta 134, 448–452.
Luo, Z.T., Lu, Y., Somers, L.A., Johnson, A.T.C., 2009. J. Am. Chem. Soc. 131, 898–899.
Manjunatha, R., Nagaraju, D.H., Suresh, G.S., Melo, J.S., D'Souza, S.F., Venkatesha, T. V., 2011. J. Electroanal. Chem. 651, 24–29.
Mariutti, L.R.B., Nogueira, G.C., Bragagnolo, N., 2008. J. Agric. Food Chem. 56, 2913–2918.
Odo, J., Inoguchi, M., Ohira, S., Tsukikawa, S., Aramaki, M., Matsuhama, S., Taito, M., Takayama, A., 2013. Anal. Sci. 29, 1041–1048.
Ram, M.K., Bertoncello, P., Ding, H., Paddeu, S., Nicolini, C., 2001. Biosens. Bioelectron. 16, 849–856.
Ruecha, N., Rangkupan, R., Rodthongkum, N., Chailapakul, O., 2014. Biosens. Bioelectron. 52, 13–19.
Shi, X.D., Li, M.Z., Ye, C.Q., Shen, W.Z., Wen, Y.Q., Chen, L.F., Yang, Q., Shi, L., Jiang, L., Song, Y.L., 2013. Laser Photonics Rev. 7, L39–L43.
Shin, H., Kim, K.K., Benayad, A., Yoon, S., Park, H.K., Jung, I., Jin, M.H., Jeong, H., Kim, J.M., Choi, J., Lee, Y.H., 2009. Adv. Funct. Mater. 19, 1987–1992.
Smith, A.M., Mancini, M.C., Nie, S., 2009. Nat. Nanotechnol. 4, 710–711.
Stewart, A.J., O'Reilly, E.J., Moriarty, R.D., Bertoncello, P., Keyes, T.E., Forster, R.J., Dennany, L., 2015. Electrochim. Acta 157, 8–14.
Vennerberg, D.C., Quirino, R.L., Jang, Y.C., Kessler, M.R., 2014. ACS Appl. Mater. Interfaces 6, 1835–1842.
Wang, K., Liu, Q., Wu, X.Y., Guan, Q.M., Li, H.N., 2010. Talanta 82, 372–376.
Wang, J., Han, H.Y., 2013. Rev. Anal. Chem. 32, 91–101.
Wang, X.F., Zhou, Y., Xu, J.J., Chen, H.Y., 2009. Adv. Funct. Mater 19, 1444–1450.
Wang, X.Y., Yang, Y., Gao, H.W., 2014. J. Lumin. 156, 229–234.
Wei, H., Wang, E.K., 2008. TrAC Trends Anal. Chem. 27, 447–459.
Wei, W., Zhou, J., Li, H.N., Yin, L.H., Pu, Y.P., Liu, S.Q., 2013. Analyst 138, 3253–3258.
Weng, J.F., Song, X.T., Li, L., Qian, H.F., Chen, K.Y., Xu, X.M., Cao, C.X., Ren, J.C., 2006. Talanta 70, 397–402.
Wu, P., Hou, X.D., Xu, J.J., Chen, H.Y., 2014a. Chem. Rev. 114, 11027–11059.
Wu, X.P., Chai, Y.Q., Yuan, R., Zhong, X., Zhang, J.J., 2014b. Electrochim. Acta 129, 441–449.
Yeh, M.H., Lin, L.Y., Sun, C.L., Leu, Y.A., Tsai, J.T., Yeh, C.Y., Vittal, R., Ho, K.C., 2014. J. Chem. Phys. 118, 16626–16634.
Zhang, C.Y., Wang, L., Wang, A.M., Zhang, S.Y., Mao, C.J., Song, J.M., Niu, H.L., Jin, B.K., Tian, Y.P., 2014b. Appl. Surf. Sci. 315, 22–27.
Zhang, H., Zhou, Z., Yang, B., 2003. J. Phys. Chem. B 107, 8–13.
Zhang, J.J., Wang, W.T., Chen, S.H., Ruo, Y., Zhong, X., Wu, X.P., 2014a. Biosens. Bioelectron. 57, 71–76.
Zhang, M.H., Yuan, R., Chai, Y.Q., Chen, S.H., Zhong, H.A., Wang, C., Cheng, Y.F., 2012. Biosens. Bioelectron. 32, 288–292.
Zhao, C.Z., Wan, L., Jiang, L., Wang, Q., Jiao, K., 2008. Anal. Biochem. 383, 25–30.